Nonlinear Estimation and Control of Bending Soft Pneumatic Actuators Using Feedback Linearization and UKF

Matheus S. Xavier, Andrew J. Fleming, and Yuen Kuan Yong

***Abstract*—In this article, we combine nonlinear estimation and control methods for precise bending angle control in soft pneumatic actuators driven by a pressure source and single low-cost ON/OFF solenoid valve. First, a complete model for the soft actuator is derived, which includes both the motion and pressure dynamics. An unscented Kalman filter (UKF) is used to estimate the velocity state and filter noisy measurements from a pressure sensor and an embedded resistive flex sensor. Then, a feedback linearization approach is used with pole placement and linear quadratic regulator (LQR) controllers for bending angle control. To compensate for model uncertainties and improve reference tracking, integral action is incorporated to both controllers. The closed-loop performance of the nonlinear estimation and control approach is experimentally evaluated with a soft pneumatic network actuator. The simulation and experimental results show that the UKF provides accurate state estimation from noisy sensor measurements. The results demonstrate the effectiveness and robustness of the proposed observer-based nonlinear controllers for bending angle trajectory tracking.**

***Index Terms*—Nonlinear control, soft pneumatic actuators, soft robotics, state estimation.**

I. Introduction

SOFT robots are continuum robots composed of highly deformable and compliant materials. Soft robots show high dexterity and safety, are physically resilient, and can adapt to delicate objects and environments due to their conformal deformation [1]. The most popular category of soft actuator is the soft pneumatic actuator [2], for which pressure control is usually achieved by regulating the duty cycle of solenoid valves [3], [4].

Currently, the model-based dynamic controllers for soft pneumatic actuators are still in their nascent stage [3], [4]. The strong nonlinearities in soft actuators and their complex geometries are the key challenges in developing accurate mathematical models [5], [6]. Analytical models for bending soft actuators have been developed using the piecewise constant curvature approach, the Euler–Bernoulli beam equation and the theory of Cosserat rods [5], [7]. A simpler method toward system modeling and controller design uses an empirical approach with energy-based inspiration to derive lumped parameter models from which the motion dynamics of a bending actuator can be approximated as a lumped second-order dynamic equation [8], [9], where the constant model parameters can be determined by curve fitting [3], [9] or system identification with a periodic input signal [4], [10].

Using this second-order model, sliding mode controllers are developed in [9], [11], [12] to control the bending angle of soft actuators governed by high-speed ON/OFF solenoid valves. A sliding mode controller with a static mapping function to create a feedforward-augmented sliding mode controller is proposed in [9]. A model reference adaptive controller augmented by a feedforward inverse dynamic controller is used in [3] to demonstrate the versatility of the proposed control approach. Sliding mode controllers using a dynamic model have also been proposed in [13]–[15], whereas a proportional derivative (PD) controller with a scheme based on cascade neural networks compensates uncertainties in a robot manipulator [16]. Alternatively, adaptive fuzzy-sliding mode [17] and energy-based [18] nonlinear controllers have been proposed for pneumatic artificial muscles using dynamic models derived using Lagrange's method. Energy-based controllers for soft pneumatic actuators using the interconnection and damping assignment passivity-based control methodology have been used in [19] and [20].

Regardless of the soft actuator design, pressure control plays a major role in the overall performance of soft robots [3], [21]. Nevertheless, few works have considered both the motion and pressure dynamics in the development of control strategies for the bending angle of soft actuators. An adaptive robust controller is proposed in [22], and a feedback linearization approach is used in [23]. In [24], backstepping and sliding mode controllers are proposed using a second-order model with nonlinear parameters. A robust backstepping control was shown to provide better tracking performance in comparison to PID control for square wave and sinusoidal references in [4].

Bending angle closed-loop control requires sensors to reconstruct the final pose of the soft actuator [25]. Embedded

Manuscript received December 17, 2021; revised February 10, 2022; accepted February 25, 2022. Recommended by Technical Editor Xinkai Chen and Senior Editor Xiang chen. *(Corresponding author: Matheus S. Xavier.)*

The authors are with the Precision Mechatronics Laboratory, School of Engineering, University of Newcastle, Callaghan, NSW 2308, Australia (e-mail: Matheus.Xavier@uon.edu.au; andrew.fleming@newcastle.edu.au; yuenkuan.yong@newcastle.edu.au).

Color versions of one or more figures in this article are available at https://doi.org/10.1109/TMECH.2022.3155790.

Digital Object Identifier 10.1109/TMECH.2022.3155790

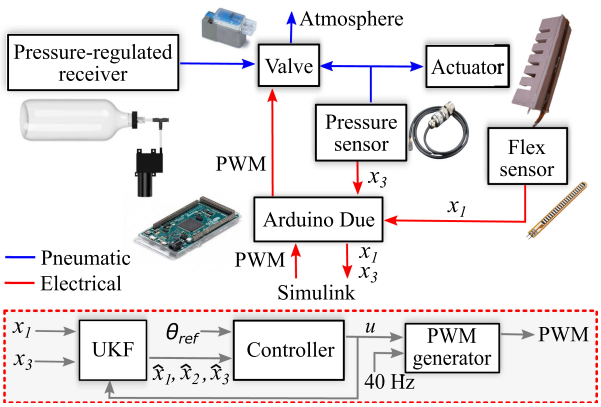

Fig. 1. Pneumatic system with 3/2 valve and pressure-regulated receiver. The bending angle of the actuator is regulated by controlling the duty cycle of the valve with a 40 Hz PWM signal. The control law u is developed using a nonlinear controller with estimated variables from the UKF. The dotted red box illustrates the implementation of the control and estimation strategies in Simulink.

sensing strategies have been proposed using commercial flex sensors [4], [25], inclinometers [22], optical waveguide sensors [12], liquid conductors [26], and magnetic sensors [11]. A data-driven approach can be used to estimate and control the bending angle of soft actuators using a static model with measurements from pressure and resistive flex sensors [27]. In this case, simple empirical models are used to predict the bending angle of soft actuators at different operating conditions but do not include the soft actuator dynamics. Extended Kalman filters have been used in [28] and [29] to estimate the curvature of soft bending actuators using quasi-static state-space models with measurements from an embedded flex sensor. These filters, however, disregard the motion dynamics of the soft robot and have not been employed for control purposes.

Angular velocity is generally required in control laws for fast closed-loop bending control. Angular velocity in rigid robots can be measured by solid-state sensors, such as tachometers, speedometers, or gyroscopes, but these are not directly applicable to soft robotics [30], [31]. As an alternative to velocity sensing, an observer-based adaptive sliding mode controller using a dynamic model based on the Euler–Lagrange method is proposed in [31] to estimate the velocity information and track-desired trajectories.

In this article, we combine nonlinear control and estimation methods for precise bending control of soft actuators using a model that includes both the motion and pressure dynamics. An unscented Kalman filter (UKF) is used to estimate the angular velocity and condition noisy measurements from the flex and pressure sensors. Following state estimation, the feedback linearization control law is developed, which allows the application of linear state-based control methods. In this work, we combine feedback linearization with pole placement using Ackermann's formula and linear quadratic regulator (LQR) controllers. To introduce robustness to model uncertainty and improve tracking performance, both controllers are augmented with integral action. The observer-based nonlinear controllers are implemented on a pneumatic network soft actuator with a pneumatic system

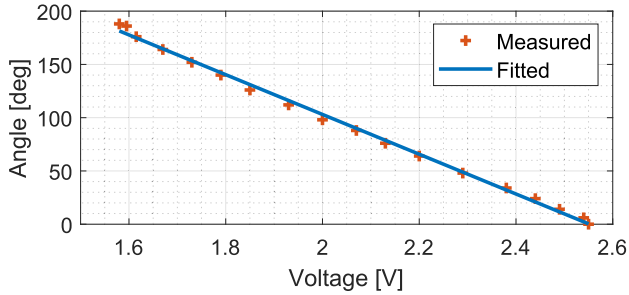

Fig. 2. Experimental data and curve fitting of flex sensor.

comprised of a single solenoidON/OFFvalve and a pressure-regulated receiver. The effectiveness of the proposed method is verified by simulation and experimental trajectory tracking results.

II. Modeling

As shown in Fig. 1, the pneumatic system in this work comprises of a single high-speed 3-way, 2-position ON/OFF valve (3/2 valve), diaphragm pump, and pressure sensors for feedback control. An air receiver is employed to improve response speed and efficiency while minimizing the peak pump flow rate. The inlet port of the valve is connected to the receiver, the outlet port is connected to the soft actuator. Bending angle control is performed by controlling the duty cycle of the pulsewidth modulation (PWM) wave into the valve. The duty cycle is determined using feedback linearization with estimated variables from the UKF based on measurements from the pressure and flex sensors.

A. Motion Dynamics

As described in [3], [8], and[9], the dynamic behavior of a bending soft actuator under a constant input can be approximated as a lumped second-order dynamic equation

$$\theta(t) = C_1 e^{(-t/\tau_1)} + C_2 e^{(-t/\tau_2)} + C_0 \tag{1}$$

where θ is the bending angle of the actuator, t is time, C_0, C_1, and C_2 are constant coefficients, and τ_1 and τ_2 are the time constants. Consequently, the dynamic response of the soft actuator can be described using a second-order transfer function

$$\frac{\theta(s)}{P(s)} = \frac{b_0}{s^2 + a_1 s + a_0} \tag{2}$$

where P is the input pressure in relative kPa.

To characterize the resistive flex sensor, a custom-made 60 mL syringe pump [32] is used to pressurize the soft actuator while recording the motion using a video camera with 60 frames per second. The change of resistance of the flex sensor is converted to voltage measurements using a voltage divider and a buffer amplifier (LM324). The software Kinovea is then used to measure the bending angles. The sensor readings and the fitted model for the flex sensor are shown in Fig. 2.

Step responses for a range of input pressure levels are shown in Fig. 3. In this work, a second-order model is employed to describe the motion dynamics of the soft actuator since it

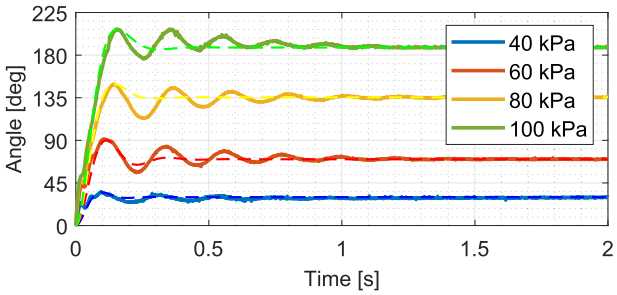

Fig. 3. Soft actuator step responses with pressures ranging from 40 kPa to 100 kPa. The solid lines are the experimental data and the dashed lines are the fitted second-order models.

TABLE I
IDENTIFIED SECOND-ORDER PARAMETERS FOR SOFT ACTUATION MOTION DYNAMICS WITH A RANGE OF INPUT PRESSURES

Parameter	40 kPa	60 kPa	80 kPa	100 kPa
b_0	1043	1007	1211	1165
a_1	34.94	23.61	31.39	29.25
a_0	1390	863.1	715.7	619.5

offers a good tradeoff between model accuracy and control complexity [4], [12], [22]. The model parameters are obtained using the percent overshoot and peak time of each response to find the damping ratio and natural frequency of the second-order model [33], which are then converted to the constants in (2). The identified parameters are presented in Table I, which are specific to our bending soft pneumatic network actuator. It can be observed that there is parameter dependency on the input pressure levels. In this work, the coefficients for an input pressure of 80 kPa are used for control and robustness is used to deal with model uncertainty.

B. Pressure Dynamics

Two fundamental equations are used to model the air pressure dynamics of the pneumatic system. The continuity equation (conservation of mass) with a polytropic gas law is used to model the actuator pressurization and the valve model ANSI/(NFPA)T3.21.3 is used to characterize the flow rate during charging and discharging.

The continuity equation is given by [34]

$$\rho_i Q_i - \rho_o Q_o = \frac{d}{dt}(\rho V) \tag{3}$$

where ρ_i and Q_i are the input density and flow rate, ρ_o and Q_o are the output density and flow rate, and ρ and V are the fluid density and volume of the control volume. If a mean density is assumed throughout, i.e., $\rho_i = \rho_o = \rho$ and recalling the definition of the bulk modulus (β) of a compressible fluid, $\beta = -V\frac{dP}{dV} \Rightarrow \frac{d\rho}{\rho} = \frac{dP}{\beta}$, then

$$Q_i - Q_o = \frac{dV}{dt} + \frac{V}{\beta}\frac{dP}{dt} \tag{4}$$

where $\frac{dV}{dt}$ corresponds to the boundary deformation term and $\frac{V}{\beta}\frac{dP}{dt}$ is the fluid compressibility term. Using a polytropic gas law, $\frac{P}{\rho^\gamma} = \text{const} \rightarrow \beta = \gamma P$, where γ is the polytropic index. For an isothermal process, $\gamma = 1$, while for an isentropic process (adiabatic and reversible), $\gamma = k = c_p/c_v = 1.4$ [35].

Using the valve model ANSI/(NFPA)T3.21.3, the volumetric flow rate Q (L/s) through a valve is

$$Q = \frac{114.5 u C_v \sqrt{P_{\text{low}} \Delta P}}{\sqrt{T_{\text{high}}}} \tag{5}$$

where $\Delta P = P_{\text{high}} - P_{\text{low}}$, P_{high}, and P_{low} are the absolute upstream and downstream pressures (bar), u is the duty cycle of the PWM signal applied to the valve, C_v is the flow coefficient and T_{high} is the upstream temperature (K).

In this work, the soft actuators are modeled as constant volume chambers, which is reasonable for actuators with low levels of ballooning, including fiber-reinforced actuators and fast pneumatic network actuators [5], [22]. Consequently, the boundary deformation term is set to zero in (4), which yields

$$\frac{dP_A}{dt} = \frac{\gamma P_A}{V_A}(Q_i - Q_o) \tag{6}$$

where P_A and V_A are the pressure and volume of the actuator.

From (5)

$$Q_i = \frac{114.5 u_c C_v \sqrt{P_A(P_R - P_A)}}{\sqrt{T_R}} \tag{7}$$

$$Q_o = \frac{114.5 u_d C_v \sqrt{P_{\text{atm}}(P_A - P_{\text{atm}})}}{\sqrt{T_A}} \tag{8}$$

where u_c and u_d are the duty cycles for the charging and discharging valves, P_R is the receiver pressure, and T_R and T_A are the receiver and actuator temperatures. Here, $T_R = T_A = T = 293.15$ K.

Inserting (7) and (8) into (6) and defining $\alpha = \frac{114.5\gamma C_v}{V_A\sqrt{T}}$ yields

$$\frac{dP_A}{dt} = \alpha P_A \left(u_c \sqrt{P_A(P_R - P_A)} - u_d \sqrt{P_{\text{atm}}(P_A - P_{\text{atm}})} \right). \tag{9}$$

C. Full Model Dynamics

For pneumatic systems with a 3/2 valve, a single PWM signal is used, hence, $u_c = u$ and $u_d = (1 - u)$. Set $x_1 = \theta$, $x_2 = \dot{\theta}$, and $x_3 = P_A$, and define $c_1 = P_R$ and $c_2 = P_{\text{atm}}$ in (9), then the actuator model takes the form

$$\dot{x}_1 = x_2 \tag{10}$$

$$\dot{x}_2 = -a_0 x_1 - a_1 x_2 + 100 b_0 (x_3 - c_2) \tag{11}$$

$$\dot{x}_3 = f_3(x_3) + g_3(x_3) u \tag{12}$$

where

$$f_3(x_3) = -\alpha x_3 \sqrt{c_2(x_3 - c_2)} \tag{13}$$

$$g_3(x_3) = \alpha x_3 \left(\sqrt{x_3(c_1 - x_3)} + \sqrt{c_2(x_3 - c_2)} \right) \tag{14}$$

and all pressures are measured in absolute bar.

The bending angle and pressure are measured using the resistive flex and pressure sensors. Therefore, the outputs of the

system are defined as follows:

$$y_1 = h_1(\mathbf{x}) = x_1 \tag{15}$$

$$y_2 = h_2(\mathbf{x}) = x_3 \tag{16}$$

where $\mathbf{x} = [x_1 \;\; x_2 \;\; x_3]^T$.

III. Control Design

A. Feedback Linearization

Since $\frac{\partial h_2}{\partial x_3} \neq 0$, a linear input–output relationship for the system defined in (12) can be obtained with the control law [36]

$$u = \frac{1}{L_{g_3} h_2(x_3)} \left(-L_{f_3} h_2(x_3) + v\right) \tag{17}$$

where $L_{f_3} h_2(x_3) = \frac{\partial h_2}{\partial x_3} f_3(x_3)$ is the Lie derivative of h_2 with respect to f_3, and $L_{g_3} h_2(x_3) = \frac{\partial h_2}{\partial x_3} g_3(x_3)$ is the Lie derivative of h_2 with respect to g_3. Since $\frac{\partial h_2}{\partial x_3} = 1$, the control law becomes

$$u = \frac{1}{g_3(x_3)} \left(-f_3(x_3) + v\right) \tag{18}$$

with $f_3(x_3)$ defined in (13) and $g_3(x_3)$ in (14). Note that, since pressures are measured in absolute bar, the denominator in the abovementioned equations is nonzero, which avoids singularities in the controller. This control law renders the linear differential equation

$$\dot{x}_3 = v. \tag{19}$$

The state-space model for the entire soft actuator dynamics can be rewritten as follows:

$$\dot{\mathbf{x}} = \mathbf{A}\mathbf{x} + \mathbf{B}v \tag{20}$$

where

$$\mathbf{A} = \begin{bmatrix} 0 & 1 & 0 \\ -a_0 & -a_1 & 100b_0 \\ 0 & 0 & 0 \end{bmatrix}, \; \mathbf{B} = \begin{bmatrix} 0 \\ 0 \\ 1 \end{bmatrix}. \tag{21}$$

In addition, we define $\mathbf{C} = [1 \;\; 0 \;\; 0]$ since the bending angle θ is the variable of interest for control purposes.

B. Pole Placement and LQR Control With Integral Action

For regulation to nonzero set-points, the following error variables are defined: $\widetilde{\mathbf{x}} = \mathbf{x} - \mathbf{x_d}$ and $\widetilde{v} = v - v_d$, where $\mathbf{x_d}$ and v_d are the desired (or reference) values. The control objective becomes the minimization of the error, i.e., $\widetilde{\mathbf{x}} \to 0$ as $t \to \infty$, which implies $\mathbf{x} \to \mathbf{x_d}$ as $t \to \infty$.

Since the motion dynamics of the soft actuator are approximated by a second-order transfer function and the parameters a_0, a_1, and b_0 have uncertainty, the control law requires robustness. Moreover, robustness is required for the receiver pressure which decreases slightly during charging, and the actuator volume which increases with pressure.

To compensate for model uncertainties and improve reference tracking, integral action is introduced by augmenting the system with a state that integrates the tracking error $\dot{\sigma} = \theta_d - \theta$. Hence, the state-space model is given by [33]

$$\begin{bmatrix} \dot{\widetilde{\mathbf{x}}} \\ \dot{\sigma} \end{bmatrix} = \underbrace{\begin{bmatrix} \mathbf{A} & \mathbf{0} \\ -\mathbf{C} & 0 \end{bmatrix}}_{\mathbf{A}_I} \underbrace{\begin{bmatrix} \widetilde{\mathbf{x}} \\ \sigma \end{bmatrix}}_{\mathbf{e}} + \underbrace{\begin{bmatrix} \mathbf{B} \\ 0 \end{bmatrix}}_{\mathbf{B}_I} \widetilde{v} \tag{22}$$

and the control law is given by

$$\widetilde{v} = -\mathbf{K}\widetilde{\mathbf{x}} + k_I \sigma = -\underbrace{\begin{bmatrix} \mathbf{K} & -k_I \end{bmatrix}}_{\mathbf{K}_I} \mathbf{e}. \tag{23}$$

Therefore, the overall linear control law is

$$v = -\mathbf{K}\mathbf{x} + k_I \sigma. \tag{24}$$

In this work, the state feedback gain matrix $\mathbf{K}_I$ in the control law $\widetilde{v}$ is determined using pole placement and LQR. For the pole placement approach, $\mathbf{K}_I$ is determined using Ackermann's formula, given as follows [33]:

$$\mathbf{K}_I = \begin{bmatrix} 0 & 0 & 0 & 1 \end{bmatrix} \begin{bmatrix} \mathbf{B_I} & \mathbf{A_I B_I} & \mathbf{A_I^2 B_I} & \mathbf{A_I^3 B_I} \end{bmatrix}^{-1} \Phi(\mathbf{A_I}) \tag{25}$$

where

$$\begin{aligned} \Phi(s) &= (s - \mu_1)(s - \mu_2)(s - \mu_3)(s - \mu_4) \\ &= s^4 + \alpha_1 s^3 + \alpha_2 s^2 + \alpha_3 s + \alpha_4 \end{aligned} \tag{26}$$

and $\mu_1, \ldots, \mu_4$ are the desired closed-loop poles.

For the LQR approach [37], $\mathbf{K}_I$ is determined to minimize the cost functional (performance index)

$$J = \int_0^\infty \mathbf{x}^T(t)\mathbf{Q}\mathbf{x}(t) + v^T(t) R v(t) \, \mathrm{dt} \tag{27}$$

with respect to the state $\mathbf{x}$ and the control v subject to the system dynamics, where $\mathbf{Q}$ is a 4×4, symmetric, positive semidefinite matrix and R is a positive real number. The optimal state feedback gain matrix is

$$\mathbf{K}_I = R^{-1}\mathbf{B_I^T P} \tag{28}$$

where $\mathbf{P}$, a positive definite, symmetric matrix, is the solution to the algebraic Riccati equation

$$\mathbf{A_I^T P} + \mathbf{P A_I} - \mathbf{P B_I} R^{-1} \mathbf{B_I^T P} + \mathbf{Q} = \mathbf{0} \tag{29}$$

which is solved using the command *lqr* in MATLAB.

IV. Unscented Kalman Filter

In this article, an UKF is used to estimate the bending velocity and filter noisy bending angle and pressure measurements. The estimated states are then used in the observer-based nonlinear controllers, as shown in Fig. 4.

First, the state-space model in (10)–(14) is discretized using Euler's approximation to obtain a discrete-time nonlinear system given by

$$x_{k+1} = f(x_k, u_k) + w_k \tag{30}$$

$$y_k = h(x_k) + v_k \tag{31}$$

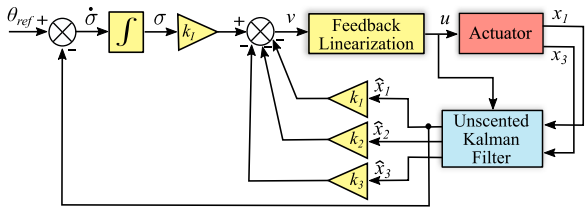

Fig. 4. Overview of a nonlinear control and estimation setup for bending angle control. The feedback gains k in the linear component of the control law v are determined using pole placement and LQR. The final control law u is determined using feedback linearization. The UKF provides the controller with the estimated variables $\widehat{x}$ based on measurements from the flex and pressure sensors.

$$w_k \sim \mathcal{N}(0, Q_k) \tag{32}$$

$$v_k \sim \mathcal{N}(0, R_k) \tag{33}$$

where it is assumed that the noise terms w_k and v_k are additive and have a Gaussian distribution. In particular, $\mathcal{N}(0, Q_k)$ indicates a multivariate normal distribution with zero mean and covariance Q_k (similarly for v_k).

The initial mean and covariance of the system are selected as $x_0^+ = [0\ \ 0\ \ P_{\text{atm}}]$ (rest position and atmospheric pressure) and $P_0^+ = 10^{-6} I_{3\times 3}$, where $I_{3\times 3}$ is the identity matrix and low values for the covariance are chosen since the initial state is known. In the following, $\widehat{x}_k^+ = E[x_k | y_1, \ldots, y_k]$ is the estimate of x_k, including all measurements up to time k, (*a posteriori* or filtered estimate) and $\widehat{x}_k^- = E[x_k | y_1, \ldots, y_{k-1}]$ is the estimate of x_k before we process the measurement at time k (*a priori* or predicted estimate), where $E(X)$ denotes the expected value of the random variable X. The UKF algorithm proceeds as follows [38], [39].

1) *Prediction update:*

a) Choose sigma points from the previous filtered Gaussian

$$\widehat{x}_{k-1}^{(i)} = \widehat{x}_{k-1}^+ + \sqrt{nP_{k-1}^+}, \quad i = 1, \ldots, n \tag{34}$$

$$\widehat{x}_{k-1}^{(n+i)} = \widehat{x}_{k-1}^+ - \sqrt{nP_{k-1}^+}, \quad i = 1, \ldots, n. \tag{35}$$

b) Propagate the sigma points through the state transition model

$$\widehat{x}_k^{(i)} = f(\widehat{x}_{k-1}^{(i)}, u_k). \tag{36}$$

c) Extract predicted mean and covariance of the states for the resulting Gaussian from the mapped sigma points

$$\widehat{x}_k^- = \frac{1}{2n} \sum_{i=1}^{2n} \widehat{x}_k^{(i)} \tag{37}$$

$$P_k^- = \frac{1}{2n} \sum_{i=1}^{2n} \left(\widehat{x}_k^{(i)} - \widehat{x}_k^-\right) \left(\widehat{x}_k^{(i)} - \widehat{x}_k^-\right)^T + Q_{k-1}. \tag{38}$$

2) *Measurement update:*

a) Choose a new set of sigma points from the predicted Gaussian

$$\widehat{x}_k^{(i)} = \widehat{x}_k^- + \sqrt{nP_k^-}, \quad i = 1, \ldots, n \tag{39}$$

$$\widehat{x}_k^{(n+i)} = \widehat{x}_k^- - \sqrt{nP_k^-}, \quad i = 1, \ldots, n. \tag{40}$$

b) Propagate the sigma points through the measurement equation to generate predicted measurements $\widehat{y}_k^{(i)}$

$$\widehat{y}_k^{(i)} = h(\widehat{x}_k^{(i)}). \tag{41}$$

c) Determine the predicted measurement $\widehat{y}_k$ at time k, the covariance of the predicted measurement P_y, and the cross covariance between $\widehat{x}_k^-$ and $\widehat{y}_k$

$$\widehat{y}_k = \frac{1}{2n} \sum_{i=1}^{2n} \widehat{y}_k^{(i)} \tag{42}$$

$$P_y = \frac{1}{2n} \sum_{i=1}^{2n} \left(\widehat{y}_k^{(i)} - \widehat{y}_k\right) \left(\widehat{y}_k^{(i)} - \widehat{y}_k\right)^T + R_k \tag{43}$$

$$P_{xy} = \frac{1}{2n} \sum_{i=1}^{2n} \left(\widehat{x}_k^{(i)} - \widehat{x}_k^-\right) \left(\widehat{y}_k^{(i)} - \widehat{y}_k\right)^T. \tag{44}$$

d) Extract the filtered mean and covariance of the states through the usual Kalman filter equations

$$K_k = P_{xy} P_y^{-1} \tag{45}$$

$$\widehat{x}_k^+ = \widehat{x}_k^- + K_k(y_k - \widehat{y}_k) \tag{46}$$

$$P_k^+ = P_k^- - K_k P_y K_k^T. \tag{47}$$

V. Simulation Results

A. Nonlinear Estimation

Simulations are developed with MATLAB/Simulink to evaluate the performance of the nonlinear control and estimation algorithms. The setup in this work employs a flex sensor for measurements of the bending angle and a pressure sensor. The performance of the UKF is compared in Fig. 5 for single sensor measurements and the combination of both sensors. The process noise covariance matrix is selected as $Q_k = \text{diag}([0.1,\ 1,\ 2 \cdot 10^{-5}])$, which was tuned by comparison with direct measurements obtained from the mathematical model in (10)–(14). The measurement noise covariances for the pressure R_P and flex R_F sensors are selected as $R_P = 2 \cdot 10^{-4}$ and $R_F = 2$, based on the noise levels of the sensor measurements. Noise is added to the simulations using a band-limited white noise block with the noise power given by $R \cdot T_s$, where R is the respective covariance and T_s is the sampling time.

The results demonstrate the robustness of the UKF in estimating state variables from noisy measurements. Using a single sensor type, reasonable estimation of the remaining states can be achieved, leading to satisfactory tracking of bending angles.

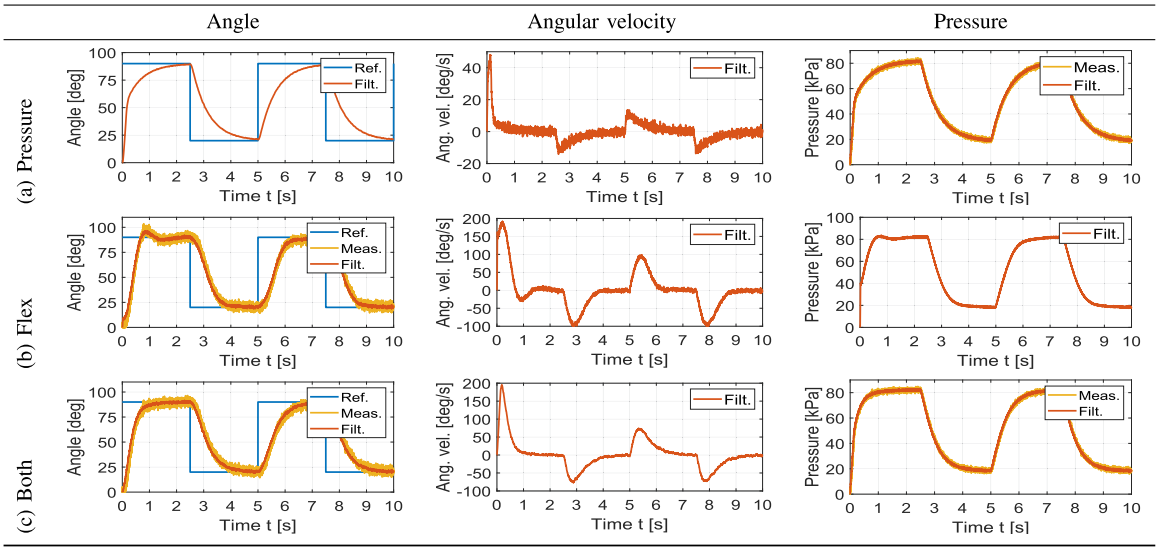

Fig. 5. Performance of the UKF for state estimation from noisy measurements. The columns show the filtered states for each of the scenarios presented by the three rows. (a) Pressure sensor alone. (b) Flex sensor alone.(c) Combination of both sensors. Feedback linearization with pole placement is used for bending angle tracking.

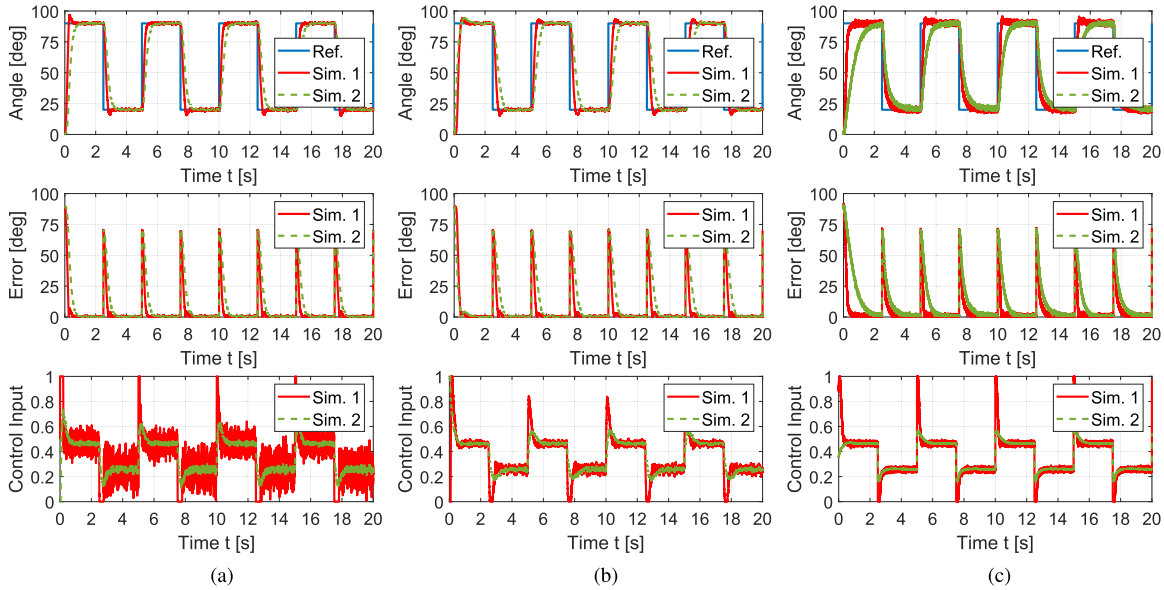

Fig. 6. Simulation results for bending angle control: comparison of tracking performance, tracking error, and control input for the proposed controllers. (a) Feedback linearization with pole placement and UKF (FL + PP + UKF). (b) Feedback linearization with LQR and UKF (FL + LQR + UKF). (c) PI control with anti-windup (PI + AW).

Nevertheless, as shown in Fig. 5(a), the angular velocity estimates from the pressure sensor alone are not sufficiently accurate for high-performance tracking. However, with both pressure and bending measurements, the estimation accuracy is significantly improved [see Fig. 5(c)], which enables high-performance reference tracking.

B. Nonlinear Control

The performance of the feedback linearization and UKF is shown in Fig. 6 for two sets of controller gains. The controllers used for the simulations in Group 2 (Sim. 2) are less aggressive than those in Group 1 (Sim. 1), which result in more sluggish responses but exhibit less overshoot, control effort, and chattering. The controller parameters and gains are listed in Table II. Both the LQR and pole placement controllers achieve sufficient tracking of the bending angle, where the LQR approach shows reduced control effort. The control effort can be further decreased, at the expense of slower response, by selecting lower values for the poles (closer to the imaginary axis) in the pole placement approach or larger values for R with LQR.

The tracking performance of the proposed nonlinear controllers is compared with PI controllers with anti-windup (AW) in Fig. 6(c). Here, AW is implemented using conditional

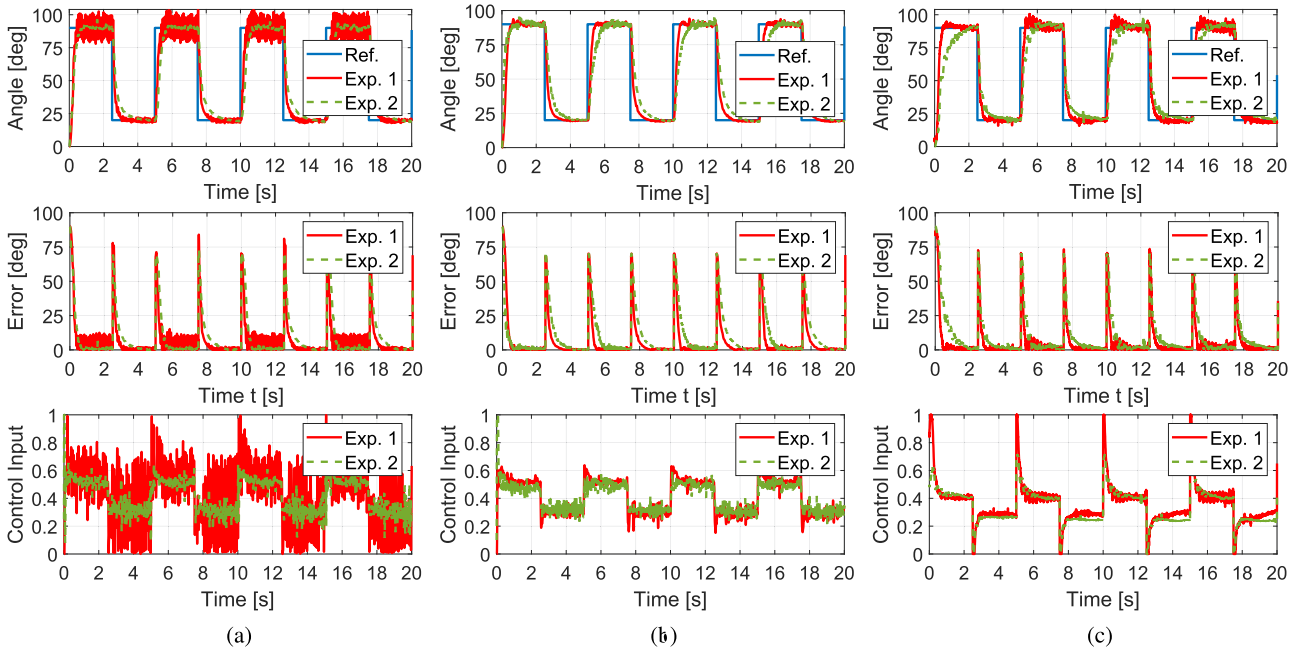

Fig. 7. Experimental results for bending angle control: comparison of tracking performance, tracking error, and control input for the proposed controllers. (a) Feedback linearization with pole placement and UKF (FL + PP + UKF). (b) Feedback linearization with LQR and UKF (FL + LQR + UKF). (c) PI control with AW (PI + AW).

TABLE II
CONTROLLER PARAMETERS AND GAINS

	Controller	Controller Parameters
Group 1: simulations and experiments	FL + PP + UKF FL + LQR + UKF PI + AW	$p = [-50\ \ -20\ \ -20\ \ -40]$ $Q = \text{diag}([10\ 1\ 1\ 30000])$, $R = 50000$ $K_P = 0.01$, $K_I = 2.8$
Group 2: simulations and experiments	FL + PP + UKF FL + LQR + UKF PI + AW	$p = [-20\ \ -8\ \ -10\ \ -30]$ $Q = \text{diag}([50\ 1\ 1\ 2000])$, $R = 50000$ $K_P = 0.005$, $K_I = 2$

The aggressive controllers in Group 1 are indicated as Sim. 1 and Exp. 1 in Figs. 6 and 7, similarly for the conservative controllers in Group 2.

integration (integrator clamping), where the integration is disabled when the duty cycle saturates [21], [40]. The PI control follows the ideal formulation, i.e., $u = -K_P\widetilde{x}_3 - K_P K_I \int \widetilde{x}_3 dt$, where $\widetilde{x}_3 = \theta - \theta_d$, and K_P and K_I are the proportional and integral gains. The performance of the PI controllers is comparable to the nonlinear control and estimation algorithms. However, as shown in Fig. 6(c), this approach is slower to respond to initial set-point changes and more sensitive to sensor noise.

VI. EXPERIMENTAL RESULTS

The pneumatic soft robotics driver proposed in [41] is connected to the Arduino Due and used to drive the diaphragm pump (KYK50BPM) and 3/2 valve (V114, SMC). The driver is also used to collect data from the pressure sensors (SEN0257, DFRobot) and the resistive flex sensor (Spectra Symbol). The control strategies are programmed using Simulink and implemented in real time on an Arduino Due with a sampling time of 5 ms.

The soft actuator used in the experimental results is a fast pneumatic network bending actuator [42] fabricated using standard molding procedures [43]. Molds are designed in Autodesk Inventor and printed using a Flashforge Inventor (Flashforge Corporation, USA). Silicone rubber (Elastosil M4601) forms the main body of the actuator with a length of 100 mm and height of 20 mm. A bottom layer of 2 mm thickness is added to the actuator, which contains the embedded flex sensor, as shown in Fig. 1.

The bending angle tracking performance and control inputs are shown in Fig. 7. Compared with the simulations, the experimental results show a larger chattering as a result of PWM switching of the ON/OFF valve and the compliance of the soft actuator. In addition, the mechanical damping produced by the hyperelastic material of the soft actuator results in reduced overshoot for the aggressive controllers.

To quantitatively compare the experimental tracking results, the following three metrics are introduced.

1) $\overline{e} = \frac{1}{N}\sum_{k=1}^{N} |e(k)|$, the average tracking error, which indicates the tracking performance.
2) $\overline{\Delta\theta} = \frac{1}{N}\sum_{k=1}^{N} |\theta(k) - \theta(k-1)|$, the average bending angle variation, which indicates the degree of chattering.
3) $\overline{u} = \frac{1}{N}\sum_{k=1}^{N} |u(k)|$, the average control input, which indicates the control effort and level of air consumption.

The performance of the control strategies is summarized in Table III. The observer-based nonlinear controllers generally outperform the PI controllers, which show larger overshoot and chattering despite the inclusion of the AW mechanism. However, the PI controllers showed lower average control inputs, which indicates increased energy efficiency. With the exception of the controller with pole placement in Group 1, the observer-based nonlinear controllers show reduced chattering owing to

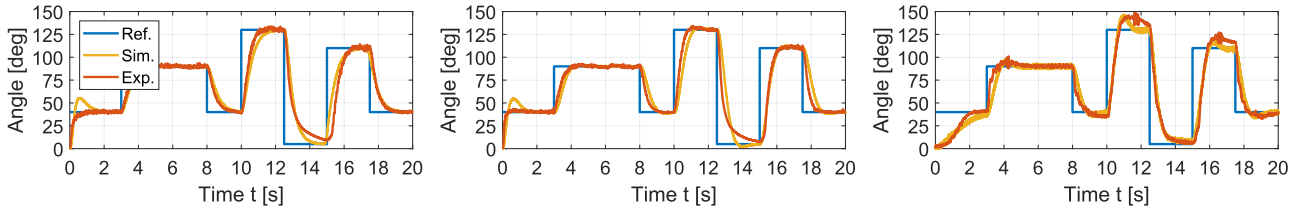

Fig. 8. Tracking performance of observer-based nonlinear controllers and PI controllers for an unstructured reference. Simulation and experimental results are shown in yellow and red, respectively. (a) FL + PP + UKF. (b) FL + LQR + UKF. (c) PI Control + AW.

TABLE III
PERFORMANCE OF CONTROL STRATEGIES

	Control	$\bar{e}$	$\overline{\Delta\theta}$	$\bar{u}$
Group 1	FL + PP + UKF	8.301	0.808	0.435
	FL + LQR + UKF	6.154	0.147	0.402
	PI + AW	6.409	0.645	0.378
Group 2	FL + PP + UKF	9.157	0.169	0.407
	FL + LQR + UKF	9.433	0.255	0.401
	PI + AW	9.590	0.516	0.359

the effectiveness of the UKF in filtering measurement noise and smoothing the effects of PWM switching. Moreover, the LQR-based controller in Group 1 has the best combination of fast response and minimum chattering.

The performance of the controllers is also evaluated for an unstructured reference input in Fig. 8. The results show that excellent tracking is achieved for the combined nonlinear control and estimation approach, which demonstrates the versatility and robustness of the feedback linearization controllers augmented with integral action. In contrast, the PI controller is slower to respond and exhibits overshoot for large set-point changes. Moreover, the PI controller is more sensitive to sensor noise, as shown by the spikes in Fig. 8(c).

VII. CONCLUSION

This article presents nonlinear estimation and control strategies for bending angle control of soft pneumatic actuators. Feedback linearization control laws are developed with pole placement and LQR approaches using filtered states from an UKF. The motion dynamics of the soft actuators are modeled using a second-order transfer function. Due to the model reduction and parameter uncertainty, both controllers are augmented with integral action to increase robustness and improve reference tracking.

The UKF was used to estimate the angular velocity state and filter noise from the pressure and resistive flex sensors. The proposed observer-based nonlinear controllers achieve excellent bending angle tracking performance and outperformed PI controllers, especially for unstructured references and large set-point changes. The feedback linearization approach with an LQR controller and UKF showed accurate and robust bending angle control with fast response and minimum chattering. Future work includes investigating the performance of observer-based nonlinear controllers with alternative embedded sensing technologies for more complex motions and the development of nonlinear system identification techniques to better characterize the motion dynamics of soft pneumatic actuators.

REFERENCES

[1] C. Majidi, "Soft-matter engineering for soft robotics," *Adv. Mater. Technol.*, vol. 4, no. 2, 2019, Art. no. 1800477.
[2] J. Walker *et al.*, "Soft robotics: A review of recent developments of pneumatic soft actuators," *Actuators*, vol. 9, no. 1, 2020, Art. no. 3.
[3] E. H. Skorina, M. Luo, W. Tao, F. Chen, J. Fu, and C. D. Onal, "Adapting to flexibility: Model reference adaptive control of soft bending actuators," *IEEE Robot. Autom. Lett.*, vol. 2, no. 2, pp. 964–970, Apr. 2017.
[4] T. Wang, Y. Zhang, Z. Chen, and S. Zhu, "Parameter identification and model-based nonlinear robust control of fluidic soft bending actuators," *IEEE/ASME Trans. Mechatronics*, vol. 24, no. 3, pp. 1346–1355, Jun. 2019.
[5] M. S. Xavier, A. J. Fleming, and Y. K. Yong, "Finite element modeling of soft fluidic actuators: Overview and recent developments," *Adv. Intell. Syst.*, vol. 3, no. 2, 2021, Art. no. 2000187.
[6] C. Tawk and G. Alici, "Finite element modeling in the design process of 3D printed pneumatic soft actuators and sensors," *Robotics*, vol. 9, no. 3, 2020, Art. no. 52.
[7] B. Gorissen, D. Reynaerts, S. Konishi, K. Yoshida, J.-W. Kim, and M. De Volder, "Elastic inflatable actuators for soft robotic applications," *Adv. Mater.*, vol. 29, no. 43, 2017, Art. no. 1604977.
[8] C. Onal and D. Rus, "Autonomous undulatory serpentine locomotion utilizing body dynamics of a fluidic soft robot," *Bioinspiration Biomimetics*, vol. 8, no. 2, 2013, Art. no. 026003.
[9] E. H. Skorina, M. Luo, S. Ozel, F. Chen, W. Tao, and C. D. Onal, "Feedforward augmented sliding mode motion control of antagonistic soft pneumatic actuators," in *Proc. IEEE Int. Conf. Robot. Autom*, 2015, pp. 2544–2549.
[10] A. H. Khan and S. Li, "Sliding mode control with PID sliding surface for active vibration damping of pneumatically actuated soft robots," *IEEE Access*, vol. 8, pp. 88793–88800, 2020.
[11] M. Luo *et al.*, "Toward modular soft robotics: Proprioceptive curvature sensing and sliding-mode control of soft bidirectional bending modules," *Soft Robot.*, vol. 4, no. 2, pp. 117–125, 2017.
[12] W. Chen, C. Xiong, C. Liu, P. Li, and Y. Chen, "Fabrication and dynamic modeling of bidirectional bending soft actuator integrated with optical waveguide curvature sensor," *Soft Robot.*, vol. 6, no. 4, pp. 495–506, 2019.
[13] J. de Jesús Rubio *et al.*, "Adapting h-infinity controller for the desired reference tracking of the sphere position in the maglev process," *Informat. Sci.*, vol. 569, pp. 669–686, 2021.
[14] L. A. Soriano *et al.*, "Optimization of sliding mode control to save energy in a SCARA robot," *Mathematics*, vol. 9, no. 24, 2021, Art. no. 3160.
[15] S. Ibrahim, J. C. Krause, A. Olbrich, and A. Raatz, "Modeling and reconstruction of state variables for low-level control of soft pneumatic actuators," *Front. Robot. AI*, vol. 8, 2021, Art. no. 557830.
[16] L. A. Soriano, E. Zamora, J. Vazquez-Nicolas, G. Hernández, J. A. Barraza Madrigal, and D. Balderas, "PD control compensation based on a cascade neural network applied to a robot manipulator," *Front. Neurorobot.*, vol. 14, 2020, Art. no. 577749.

[17] D. Liang, N. Sun, Y. Wu, G. Liu, and Y. Fang, "Fuzzy-sliding mode control for humanoid arm robots actuated by pneumatic artificial muscles with unidirectional inputs, saturations, and dead zones," *IEEE Trans. Ind. Inform.*, vol. 18, no. 5, pp. 3011–3021, May 2022.

[18] D. Liang, N. Sun, Y. Wu, Y. Chen, Y. Fang, and L. Liu, "Energy-based motion control for pneumatic artificial muscle-actuated robots with experiments," *IEEE Trans. Ind. Electron.*, vol. 69, no. 7, pp. 7295–7306, Jul. 2022.

[19] E. Franco, A. G. Casanovas, and A. Donaire, "Energy shaping control with integral action for soft continuum manipulators," *Mech. Mach. Theory*, vol. 158, 2021, Art. no. 104250.

[20] E. Franco, T. Ayatullah, A. Sugiharto, A. Garriga-Casanovas, and V. Virdyawan, "Nonlinear energy-based control of soft continuum pneumatic manipulators," *Nonlinear Dyn.*, vol. 106, no. 1, pp. 229–253, 2021.

[21] M. S. Xavier, A. J. Fleming, and Y. K. Yong, "Design and control of pneumatic systems for soft robotics: A simulation approach," *IEEE Robot. Autom. Lett.*, vol. 6, no. 3, pp. 5800–5807, Jul. 2021.

[22] C. Chen, W. Tang, Y. Hu, Y. Lin, and J. Zou, "Fiber-reinforced soft bending actuator control utilizing On/Off valves," *IEEE Robot. Autom. Lett.*, vol. 5, no. 4, pp. 6732–6739, Oct. 2020.

[23] V. Falkenhahn, A. Hildebrandt, R. Neumann, and O. Sawodny, "Dynamic control of the bionic handling assistant," *IEEE/ASME Trans. Mechatron.*, vol. 22, no. 1, pp. 6–17, Feb. 2016.

[24] C. Chen and J. Zou, "Adaptive robust control of soft bending actuators: An empirical nonlinear model-based approach," *J. Zhejiang Univ. Sci. A*, vol. 22, no. 9, pp. 681–694, 2021.

[25] G. Gerboni, A. Diodato, G. Ciuti, M. Cianchetti, and A. Menciassi, "Feedback control of soft robot actuators via commercial flex bend sensors," *IEEE/ASME Trans. Mechatronics*, vol. 22, no. 4, pp. 1881–1888, Aug. 2017.

[26] R. K. Kramer, C. Majidi, R. Sahai, and R. J. Wood, "Soft curvature sensors for joint angle proprioception," in *Proc. IEEE/RSJ IEEE Int. Conf. Intell. Robots Syst.*, 2011, pp. 1919–1926.

[27] K. Elgeneidy, N. Lohse, and M. Jackson, "Bending angle prediction and control of soft pneumatic actuators with embedded flex sensors-a data-driven approach," *Mechatronics*, vol. 50, pp. 234–247, 2018.

[28] J. Y. Loo, K. C. Kong, C. P. Tan, and S. G. Nurzaman, "Non-linear system identification and state estimation in a pneumatic based soft continuum robot," in *Proc. IEEE Conf. Control Technol. Appl.*, 2019, pp. 39–46.

[29] J. Y. Loo, Z. Y. Ding, E. Davies, S. G. Nurzaman, and C. P. Tan, "Curvature and force estimation for a soft finger using an EKF with unknown input optimization," *IFAC-PapersOnLine*, vol. 53, no. 2, pp. 8506–8512, 2020.

[30] G. Cao, B. Huo, L. Yang, F. Zhang, Y. Liu, and G. Bian, "Model-based robust tracking control without observers for soft bending actuators," *IEEE Robot. Autom. Lett.*, vol. 6, no. 3, pp. 5175–5182, Jul. 2021.

[31] G. Cao, Y. Liu, Y. Jiang, F. Zhang, G. Bian, and D. H. Owens, "Observer-based continuous adaptive sliding mode control for soft actuators," *Nonlinear Dyn.*, vol. 105, pp. 1–16, 2021.

[32] M. S. Xavier, A. J. Fleming, and Y. K. Yong, "Image-guided locomotion of a pneumatic-driven peristaltic soft robot," in *Proc. IEEE Int. Conf. Rob. Biomimetics*, 2019, pp. 2269–2274.

[33] K. Ogata and Y. Yang, *Modern Control Engineering*. Englewood Cliffs, NJ, USA: Prentice Hall, 2010.

[34] J. Watton, *Fluid Power Systems: Modeling, Simulation, Analog and Microcomputer Control*. Englewood Cliffs, NJ, USA: Prentice-Hall, 1989.

[35] M. S. Xavier, A. J. Fleming, and Y. K. Yong, "Modeling and simulation of pneumatic sources for soft robotic applications," in *Proc. IEEE/ASME Int. Conf. Adv. Intell. Mechatronics*, 2020, pp. 916–921.

[36] H. J. Marquez, *Nonlinear Control Systems: Analysis and Design*. Hoboken, NJ, USA: Wiley, 2003.

[37] D. S. Naidu, *Optimal Control Systems*. Boca Raton, FL, USA: CRC Press, 2002.

[38] S. Thrun, W. Burgard, and D. Fox, *Probabilistic Robotics*. Cambridge, MA, USA: MIT Press, 2005.

[39] D. Simon, *Optimal State Estimation: Kalman, H. Infinity, and Nonlinear Approaches*. Hoboken, NJ, USA: Wiley, 2006.

[40] A. Visioli, *Practical PID Control*. Berlin, Germany: Springer, 2006.

[41] T. R. Young, M. S. Xavier, A. J. Fleming, and Y. K. Yong, "A control and drive system for pneumatic soft robots: Pneusord," in *Proc. IEEE/RSJ Int. Conf. Intell. Robots Syst.*, 2021, pp. 2822–2829.

[42] B. Mosadegh *et al.*, "Pneumatic networks for soft robotics that actuate rapidly," *Adv. Funct. Mater.*, vol. 24, no. 15, pp. 2163–2170, 2014.

[43] F. Schmitt, O. Piccin, L. Barbé, and B. Bayle, "Soft robots manufacturing: A review," *Front. Robot. AI*, vol. 5, 2018, Art. no. 84.